ACS central science

http://pubs.acs.org/journal/acscii

Research Article

Room-Temperature Flexible Quasi-Solid-State Rechargeable Na−O_2 Batteries

Jiaqi Wang,[†] Youxuan Ni,[†] Junxiang Liu, Yong Lu, Kai Zhang, Zhiqiang Niu, and Jun Chen*

Cite This: *ACS Cent. Sci.* 2020, 6, 1955−1963

Read Online

ACCESS | Metrics & More | Article Recommendations | Supporting Information

ABSTRACT: Rechargeable Na−O_2 batteries have been regarded as promising energy storage devices because of their high energy density, ultralow overpotential, and abundant resources. Unfortunately, conventional Na−O_2 batteries with a liquid electrolyte often suffer from severe dendrite growth, electrolyte leakage, and potential H_2O contamination toward the Na metal anode. Here, we report a quasi-solid-state polymer electrolyte (QPE) composed of poly(vinylidene fluoride−*co*-hexafluoropropylene)−4% SiO_2−$NaClO_4$−tetraethylene glycol dimethyl ether for rechargeable Na−O_2 batteries with high performance. Density functional theory calculations reveal that the fluorocarbon chains of QPE are beneficial for Na^+ transfer, resulting in a high ionic conductivity of 1.0 mS cm^{-1}. Finite element method simulations show that the unique nanopore structure and high dielectric constant of QPE can induce a uniform distribution of the electric field during charge/discharge processes, thus achieving a homogeneous deposition of Na without dendrites. Moreover, the nonthrough nanopore structure and hydrophobic behavior resulting from fluorocarbon chains of QPE could effectively protect Na anode from H_2O erosion. Therefore, the fabricated quasi-solid-state Na−O_2 batteries exhibit an average Coulombic efficiency of up to 97% and negligible voltage decay during 80 cycles at a discharge capacity of 1000 mAh g^{-1}. As a proof of concept, flexible pouch-type Na−O_2 batteries were assembled, displaying stable electrochemical performance for ∼400 h after being bent from 0 to 360°. This work demonstrates the application of the quasi-solid-state electrolyte for high-performance flexible Na−O_2 batteries.

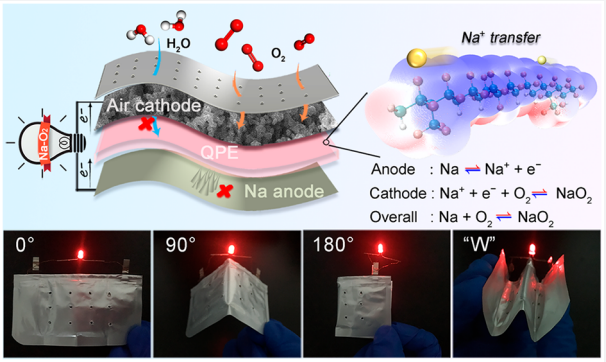

INTRODUCTION

Recently, Na−O_2 batteries have drawn considerable attention due to their high theoretical energy density (1105 Wh kg^{-1}), ultralow overpotential, and abundant resources.[1−6] However, there are several difficulties hindering the practical application of Na−O_2 batteries.[7−10] For example, Na−O_2 batteries with a Na metal anode and a liquid organic electrolyte are often plagued by dendrite growth and electrolyte leakage. A Na dendrite formed during the charging process will easily cause a short circuit.[11−16] Furthermore, the high reactivity of the Na metal anode will lead to electrolyte decomposition and Na corrosion by contaminant H_2O or O_2 from the cathode side.[17−19] In addition, due to the open systems of Na−O_2 batteries, liquid organic electrolyte is more prone to leak out or volatilize, limiting the battery life and raising safety concerns.[20−22] To promote the practical application of rechargeable Na−O_2 batteries, it is necessary to develop effective strategies to solve the aforementioned problems.

Previous works mainly focus on inhibiting Na dendrite growth in Na−O_2 batteries by alloying a three-dimensional framework and an artificial protective layer.[23−26] Although the Na dendrite can be solved to some extent, the contamination of H_2O toward the Na metal anode and the leakage of electrolyte are generally overlooked. A quasi-solid-state polymer electrolyte (QPE) has the advantages of a high conductivity, good mechanical properties, and high liquid locking ability. Once QPE has a nonthrough pore structure and hydrophobic properties to avoid Na metal erosion by H_2O, it could show great potential to simultaneously solve the aforementioned problems. Among all QPEs, a poly(vinylidene fluoride−*co*-hexafluoropropylene) (PVdF−HFP)-based QPE has attracted much attention recently due to its unique chemical and physical properties.[27−29] However, to our best knowledge, the understanding of the intrinsic properties and the role of a (PVdF−HFP)-based QPE in ion transfer are still insufficient. Unravelling the effect of QPE on ion dispersion or transfer helps to give guidance toward the design of a polymer electrolyte. In addition, there is still no report about QPE for rechargeable Na−O_2 batteries so far. Therefore, it is of vital significant to construct QPE with a special nonthrough pore

Received: June 26, 2020
Published: October 27, 2020

https://dx.doi.org/10.1021/acscentsci.0c00849
ACS Cent. Sci. 2020, 6, 1955−1963

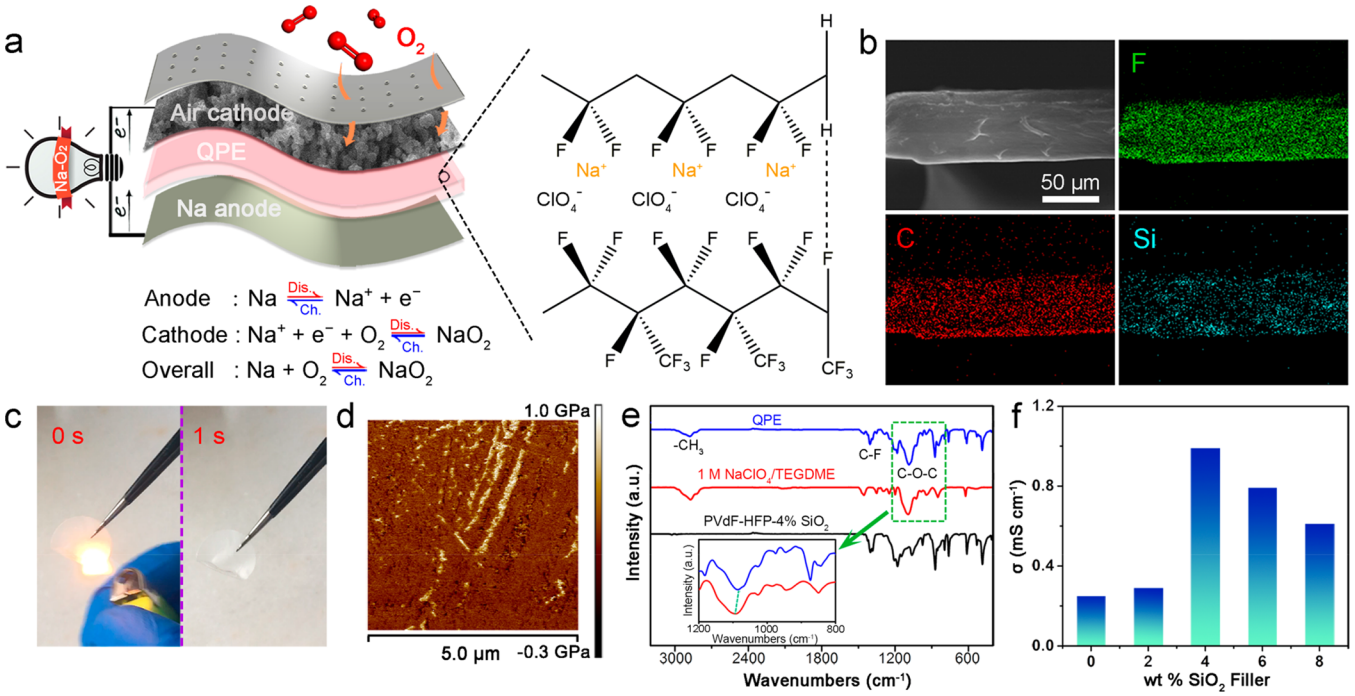

Figure 1. Structures and properties of QPE. (a) Schematic diagram of a Na−O_2 battery with a Na foil anode, QPE, and air cathode. (b) Cross-sectional SEM image of QPE and corresponding EDX mapping of F, C, and Si. (c) Inflammability test. The lighter flame temperature is ∼500 °C. (d) Young's modulus of QPE. (e) FTIR of the QPE, polymer matrix, and liquid component. (f) Ionic conductivity of QPE with different contents of nano-SiO_2 fillers.

structure, abundant hydrophobic functional groups, and the ability to disperse Na-ion flux for high-performance Na−O_2 batteries.

Herein, we report a nonflammable QPE that consists of PVdF−HFP−4% SiO_2−$NaClO_4$−tetraethylene glycol dimethyl ether (TEGDME) as an electrolyte for Na−O_2 batteries. The abundant fluorocarbon chains of QPE also play an important role in Na^+-ion transfer, resulting in a high ionic conductivity of 1.0 mS cm^{-1}. The Na dendrites can be effectively inhibited, because the unique porous structure and high dielectric constant of QPE could regulate a uniform distribution of an electric field during the charge/discharge processes, as proved by finite element method simulations. Furthermore, the hydrophobicity originated from fluorocarbon chains and the nonthrough nanopore structure of QPE could defend the Na metal anode against H_2O erosion. Additionally, the enhanced liquid locking ability of QPE avoids the possible leakage of electrolyte. As a result, Na−O_2 batteries exhibit negligible voltage decay after cycling for 80 cycles at a cutoff discharge capacity of 1000 mAh g^{-1}. Moreover, flexible Na−O_2 batteries show good cycling stability for 400 h after being bent from 0 to 360°.

RESULTS AND DISCUSSION

The configuration of a flexible quasi-solid-state Na−O_2 battery is illustrated in Figure 1a, which contains the Na metal anode, air cathode, and QPE. QPE was synthesized through the modification of a PVdF−HFP polymer matrix with a nano-SiO_2 additive and then a plasticization process by 1 M $NaClO_4$/TEGDME. The PVdF−HFP polymer matrix possesses a large amount of fluorocarbon chains, which are uniformly distributed in the matrix to make QPE hydrophobic (Figure 1b).[30] QPE has a thickness of about 60 μm and displays a smooth surface with a low roughness (Rq or average deviation) of 12.9 nm, as suggested by atomic force microscopy (AFM) (Figures S1 and S2), ensuring the intimate contact between QPE and the electrodes. In addition, different from the traditional inflammable Celgard separator, such a polymer film has good flame resistance. The combustion experiment proves that an open fire could be quickly extinguished automatically in only 1 s when it was ignited (Figure 1c). In contrast, the Celgard separator was burned out (Figure S3). Moreover, QPE possesses excellent tensile properties (Figure S4) and a high Young's modulus of about 0.5 GPa (Figure 1d), which endows it with good mechanical properties to serve as both the electrolyte and separator of flexible Na−O_2 batteries. Thermogravimetric analysis indicates that the weight ratio of TEGDME solvent in QPE is approximately 29.4%, much less than those of the Celgard separator (77.1%) and glass fiber separator (84.3%) (Figure S5). The existence of TEGDME in QPE is confirmed by Fourier transform infrared (FTIR) spectroscopy (Figure 1e). Bands at around 2871 and 1096 cm^{-1} indicate the presence of $-CH_3$ and C−O−C in TEGDME, respectively, and a band at 1400 cm^{-1} is identified as the stretching signal of C−F in a polymer matrix. The red shift of C−O−C stretching vibration frequencies could be observed due to the intermolecular force between polymer chains and TEGDME, which would effectively enhance the liquid locking ability of the polymer matrix and thus suppress the electrolyte volatilization and leakage (Figure S6).[31] The conductivity of QPE could be optimized by adjusting the weight ratio of hydrophobic fumed silica with a diameter of ∼15 nm (Figures S7 and S8). The introduction of SiO_2 fillers could lessen the crystalline region to improve the ionic conductivity of QPE. However, since SiO_2 is not conductive for Na^+, excessive additives will lower the ionic conductivity.[32−34] After optimization, the results reveal

https://dx.doi.org/10.1021/acscentsci.0c00849
ACS Cent. Sci. 2020, 6, 1955−1963

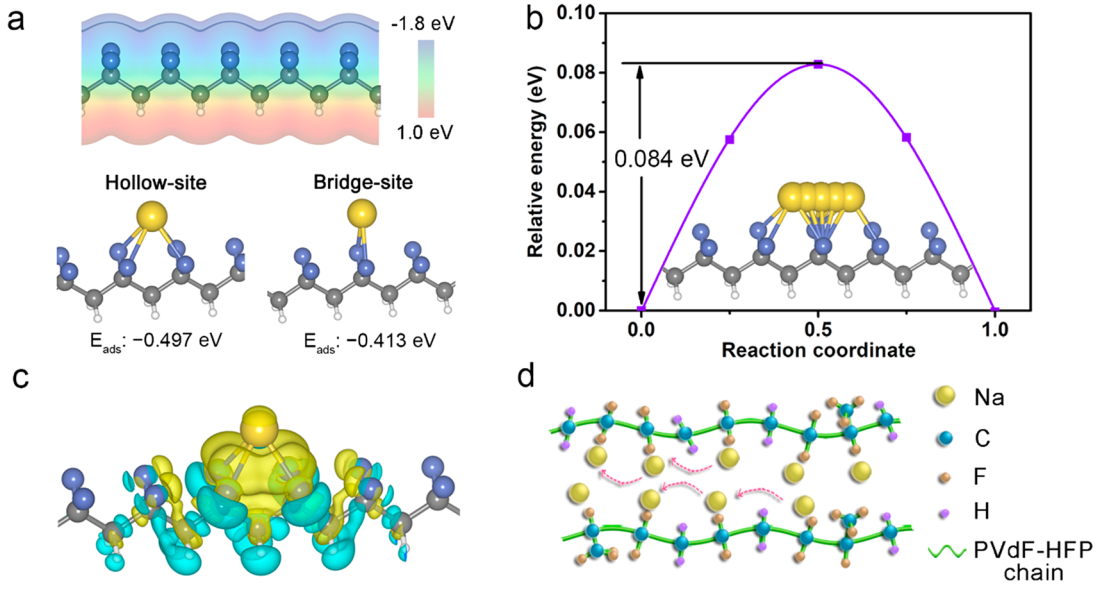

Figure 2. DFT calculations about the transfer mechanism of Na^+ ions along polymer chains. (a) Electrostatic potential map of polymer chains and adsorption sites of Na^+ ions on polymer chains. (b) Na^+-ion transfer along the polymer chains. (c) Side view of charge transfer after the adsorption of Na^+ ions. Yellow means electron accumulation, and cyan means electron depletion. The yellow, gray, blue, and white spheres represent sodium, carbon, oxygen, and hydrogen, respectively. (d) Schematic diagram of Na^+-ion transfer along polymer chains.

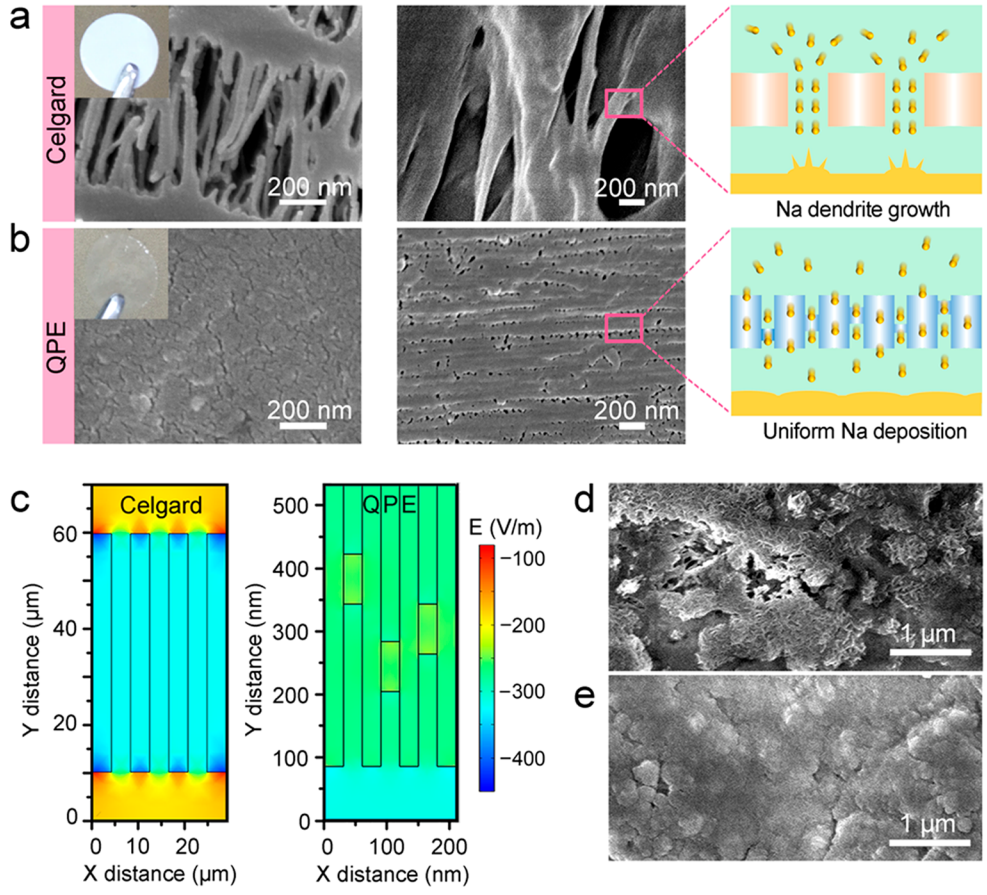

Figure 3. Redistribution and deposition behaviors of Na^+ ions through the Celgard separator and QPE. SEM images of the Celgard separator and QPE from the top and cross section, and schematic illustrations of Na^+-ion distribution of (a) the Celgard separator and (b) QPE. Insets: optical photographs of the Celgard separator and QPE. (c) Simulated electrical field distribution in the Celgard separator and QPE. For the QPE system, the color-filled map is the local enlarged image of electric field distribution. Colors in the graph represent the vertical component of electric field strength. SEM images of Na metal anodes in Na−Na symmetric cells with the (d) Celgard separator and (e) QPE after cycling for 100 h.

https://dx.doi.org/10.1021/acscentsci.0c00849
ACS Cent. Sci. 2020, 6, 1955−1963

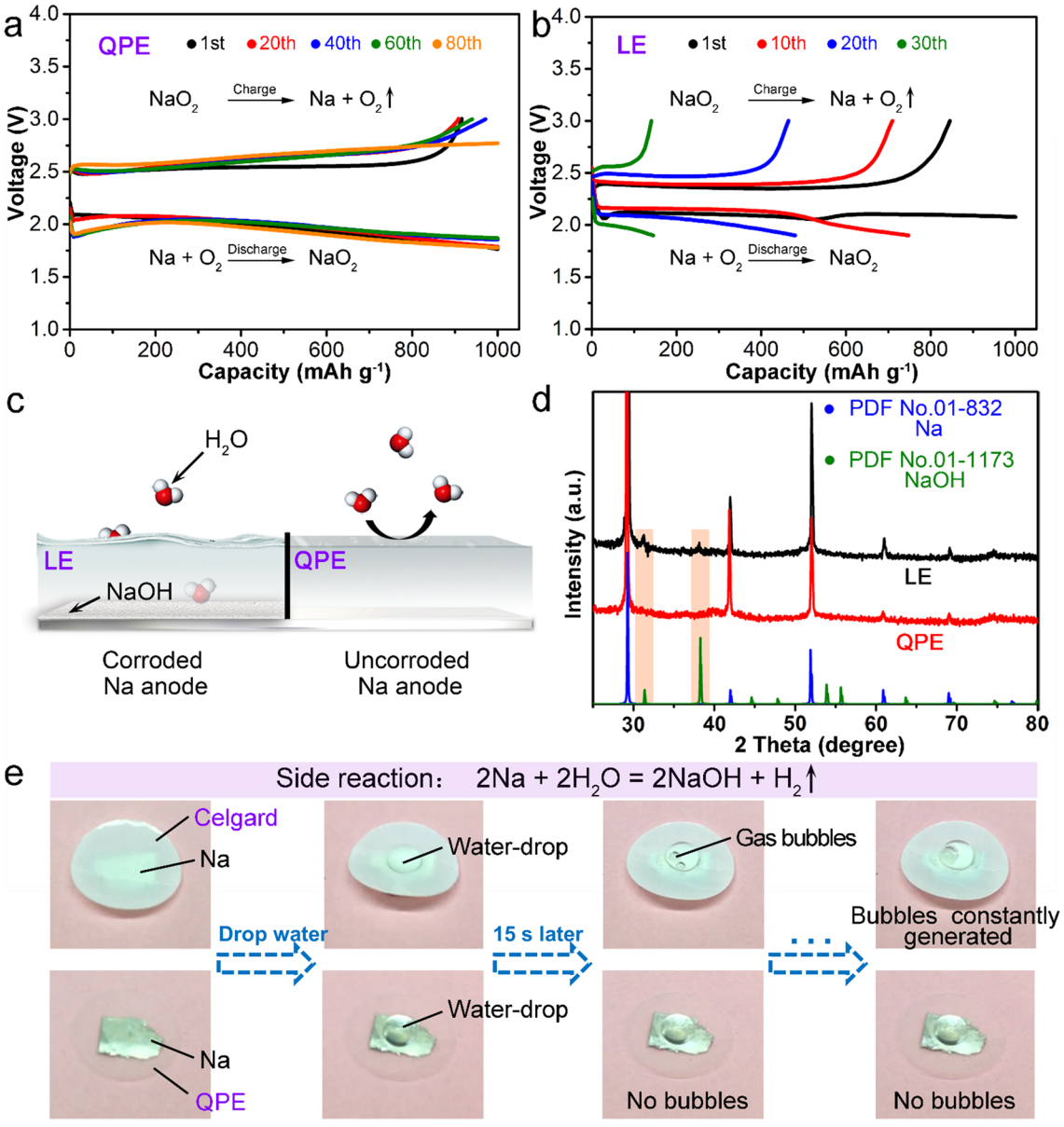

Figure 4. Electrochemical behaviors of QPE-/LE-based Na−O_2 batteries and the barrier role of QPE against water. Discharge−charge profiles of Na−O_2 batteries with (a) QPE and (b) LE. (c) Schematic representation of QPE as a barrier for H_2O to the Na anode. (d) X-ray diffraction of the Na anode in Na−O_2 batteries based on LE and QPE after 20 cycles. (e) Waterproofness of Celgard separator and QPE.

that QPE with 4 wt % SiO_2 exhibits the highest ionic conductivity of 1.0 mS cm^{-1} (Figures 1f and S9).

Although the ionic conductivity of QPE is mostly attributed to the Na^+-ion diffusion in the liquid region of QPE, the fluorocarbon chains also take part in the transfer of Na^+ ions. Considering the complexity and disorder of such copolymers, we simplified the models and focused on the interaction between adsorbed Na^+ ions and PVdF segments to understand the transportation mechanism of Na^+ ions along the polymer chains. Owing to the strong electronegativity of fluorine atoms as presented by an electrostatic potential (ESP) map (Figures 2a and S10), Na^+ ions tend to be adsorbed and transferred on the "fluorine ribbon". In our case, two adsorption sites, hollow and bridge sites, are considered as the favorable adsorption sites (Figure 2a). Hollow sites possess a larger adsorption energy of −0.497 eV, while bridge sites have a smaller one of −0.413 eV. The relative energy of adsorption system changes along with the migration of Na^+ ions along the fluorocarbon chain (Figure 2b). The migration energy barrier of Na^+ ions along the fluorocarbon chain is 0.084 eV. Such an extremely low barrier is easy to overcome. Moreover, the ab initio molecular dynamics simulation results also prove such a transfer mechanism (Figure S11). The charge transfer of Na^+ ions adsorbed on the hollow site is plotted in Figures 2c and S12, where the electrons gather around the fluorine atoms to stabilize the Na^+ ions. That indicates the interaction between the Na^+ ions and the polymer chains derives from electrostatic attraction. The charge redistribution of Na^+ ions on the bridge site is shown in Figure S13. Consequently, the adsorption is strong enough to hold Na^+ ions on the "fluorine ribbon" while the migration barrier is low enough to ensure that Na^+ ions migrate freely (Figure 2d). Considering the abundance of fluorocarbon chains, this feature would allow QPE to effectively disperse Na^+-ion flux.

https://dx.doi.org/10.1021/acscentsci.0c00849
ACS Cent. Sci. 2020, 6, 1955−1963

A conventional Celgard separator has an irregular macroporous structure, which commonly leads to the nonuniform distribution of Na^+ ions through the separator (Figure 3a) and subsequent inhomogeneous Na deposition. Unlike the Celgard separator, QPE exhibits a composite construction containing a liquid component and an ionic conductive polymer matrix with smaller and densely distributed pores (Figure S14). Furthermore, it is noted that the pore structure of QPE is nonthrough (Figure S15). In QPE, the ions could transfer across both polymer matrix and liquid component in the nanopores, resulting in a much more uniform distribution of Na^+ ions (Figure 3b). To further understand the dependence of Na deposition on the structure of separators, finite element method (FEM) simulations were performed to investigate the electric field distribution in these two systems. As shown in Figure 3c, the vertical component of electric field strength around the surface of a Celgard separator is nonuniform. In contrast, such a component varies slightly along the surface of a QPE. Notably, the actual pores are more complex and random.[35] For a visible comparison, these models are simplified to just estimate the impact of pore size and dielectric constant on electric field distribution (details in Finite Element Simulations). The electric field distribution plays an important role in Na deposition.[36,37] The more evenly distributed the electric field, the more uniform Na deposition will be. To illustrate this, Na−Na symmetric cells were assembled based on a conventional Celgard separator and QPE (Figure S16). In the case of a conventional Celgard-separator-based cell, the Na electrode was severely damaged. A large amount of mossy Na and rough cracks were observed after cycling for 100 h (Figure 3d).[38] In contrast, uniform Na deposition occurred on a Na electrode in the case of QPE (Figure 3e). These results indicate that QPE will induce a uniform electric field distribution around the surface and thus result in homogeneous Na deposition, which is different from physically suppressing Na dendrites.[39−41]

Apart from the above advantages, QPE also possesses a suitable electrochemical stability window, which is much wider than the operating window of Na−O_2 batteries (Figure S17). These properties enable QPE to act as both the separator and electrolyte for Na−O_2 batteries to achieve the feasibility of batteries. Na−O_2 batteries with QPE could operate stably with a relative low polarization (~0.5 V) and an average Coulombic efficiency of up to 97% during 80 cycles with a discharge capacity of 1000 mAh g^{-1} at 200 mA g^{-1}, and no obvious voltage decay is observed (Figure 4a). Although QPE is utilized in our case, the electrochemical performance of resultant Na−O_2 batteries is still comparable with recently reported works, as shown in Table S1. This electrochemical performance is also superior to the case of Na−O_2 batteries based on LE, which suffer severe capacity decay and dramatically increased polarization during cycling due to the degradation of a Na anode (Figures 4b, S18, and S19). Moreover, quasi-solid-state Na−O_2 batteries also exhibit satisfactory rate capacity without a significant polarization increase as the current density rises (Figure S20). Notably, the aforementioned current and capacity are based on the mass of Super P, because the capacity of carbon paper is negligible when compared with that of the Super-P-coated carbon paper (Figure S21) or carbon cloth (Figure S22).

Trace water, which may come from the impure salt hydrates or gas in the atmosphere, is extremely harmful to a Na metal anode.[42] Therefore, the waterproofness of a separator in a Na−O_2 battery system is also significant for the electrochemical performance of Na−O_2 batteries. QPE displays a hydrophobic behavior with a contact angle over 90° due to widespread hydrophobic fluorocarbon chains (Figure S23). Thus, QPE can prevent the contamination H_2O from eroding the sodium metal anode to form sodium hydroxide (Figure 4c,d). In contrast, sodium hydroxide accumulates on the surface of the Na anode due to the continuous attack of water in the LE-based Na−O_2 battery (Figure 4d). To verify this, the waterproofness of the Celgard separator and QPE was analyzed, by dropping a water drop onto metal sodium covered with a piece of a Celgard separator or QPE (Figure 4e). In less than 15 s, visible bubbles would appear in the water droplets on the Celgard separator and be generated constantly later, which corresponds to the side reaction of $2Na + 2H_2O = 2NaOH + H_2\uparrow$. On the contrary, the metal sodium covered with QPE was not corroded by water, indicating the water drop could not penetrate through QPE to contact the metal sodium. This dynamic change can be seen in Video S1. Obviously, the nonthrough pore structure and hydrophobic behavior of QPE contribute to the above stable electrochemical performance of Na−O_2 batteries. Additionally, the protective effect of QPE for Na metal in oxygen and air atmosphere is investigated (Figure S24). Compared with a Celgard separator, QPE can significantly reduce the corrosion of Na metal (Figure S25). However, there is still a long way to go in the achievement of Na−air batteries which can really operate in an air atmosphere. One of the problems is that a high content of water in air is fatal to discharge product NaO_2, since QPE cannot hinder the reaction between NaO_2 and H_2O on cathodes, even if QPE can protect the Na anode from corrosion to some extent. To demonstrate the potential applications of QPE in large-capacity Na−O_2 batteries, we fabricated a pouch-type Na−O_2 battery in a size of 10 × 10 cm^2 (Figures S26 and S27). The pouch-type battery displays a large capacity of 636.1 mAh, corresponding to 335 Wh kg^{-1} based on the total mass of the whole battery (Figures S28 and S29), which is higher than that of commercial Li-ion batteries,[43] suggesting the possibility of a large-scale application of QPE for rechargeable Na−O_2 batteries.

In order to understand the discharge/charge mechanism of QPE-based Na−O_2 batteries, the evolution of discharge products was characterized by SEM, XRD, and Raman. As Na−O_2 batteries discharged at 500 mAh g^{-1}, microsized crystalline NaO_2 cubes were formed on the surface of the Super P carbon cathode (Figure S30), which is consistent with previous reports.[44−46] The characteristic peaks of discharge product NaO_2 were observed at 32.8, 46.9, and 58.4° in the corresponding XRD patterns, which are ascribed to the (200), (220), and (222) crystal planes of NaO_2 (JCPDS card No. 89-5951; Figure S31), respectively. Then, these peaks would reversibly disappear after full charge. Furthermore, such a reversible evolution of NaO_2 was also confirmed by Raman (Figure S32), where the peak at 1156 cm^{-1} indicates the existence of NaO_2.[47] Therefore, the discharge/charge mechanism of QPE-based Na−O_2 batteries is similar to the case of LE-based Na−O_2 batteries and independent of the behavior of QPE.

As a proof of concept, we further assembled flexible pouch-type Na−O_2 batteries based on QPE. The QPE film was sandwiched between a sodium metal anode and a porous flexible carbon cloth cathode sprayed with Super P (Figure S33). Then, they were encapsulated in aluminum−plastic film

https://dx.doi.org/10.1021/acscentsci.0c00849
ACS Cent. Sci. 2020, 6, 1955−1963

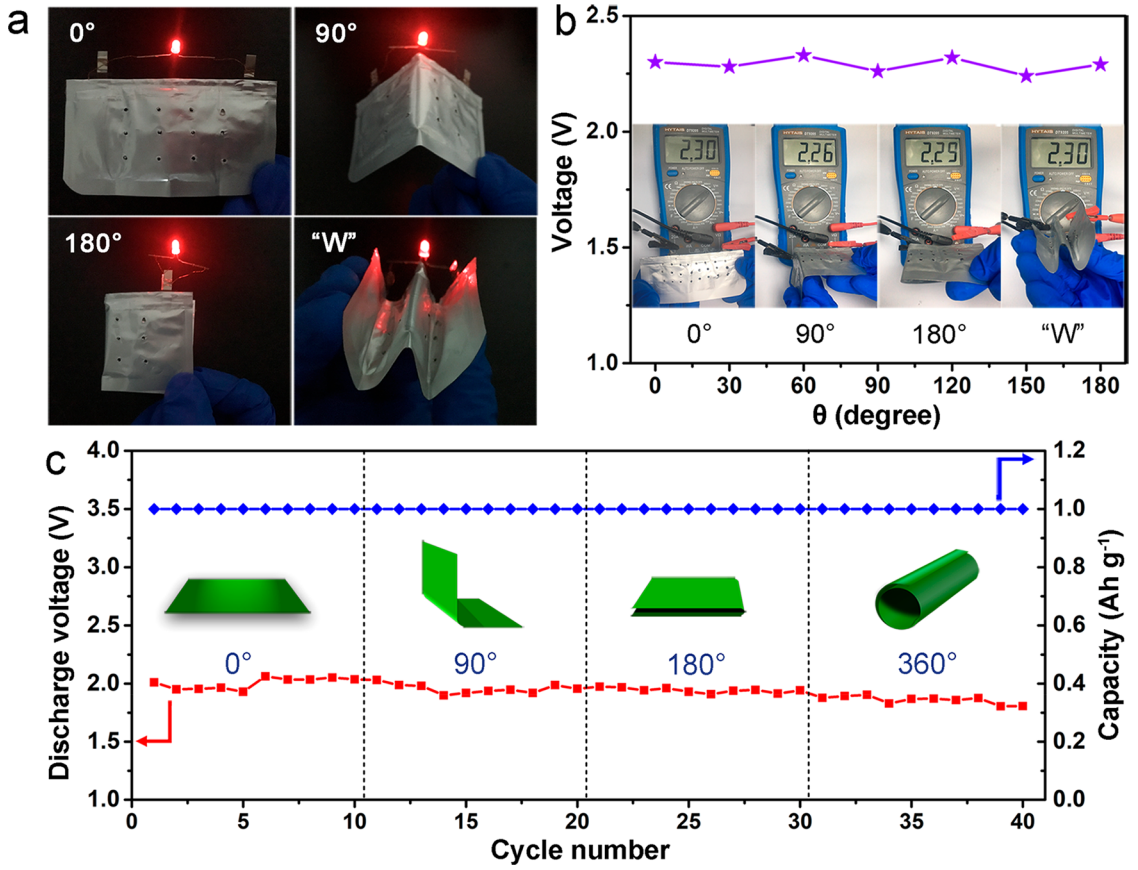

Figure 5. Configuration and electrochemical performance of flexible QPE-based Na−O_2 batteries. (a) The optical images of the LED lit by the integrated flexible Na−O_2 battery at different states. (b) Open circuit voltage of flexible Na−O_2 battery at varied folding levels. (c) Cycling performance of Na−O_2 battery under various bended and twisted conditions.

with many small holes on the cathode side, which facilitate O_2 gas diffusion. To demonstrate the electrochemical stability at different strains, the as-fabricated pouch-type Na−O_2 battery was bent and twisted into four different states. There is no structural damage in Na−O_2 batteries at these various bending and twisting states. A fatigue test of the flexible QPE-based Na−O_2 battery is shown in Figure S34. Furthermore, the red-light-emitting diode remained constantly powered with equivalent brightness under the corresponding testing conditions (Figure 5a). Moreover, the open circuit voltage of such a Na−O_2 battery device was nearly unchanged (ca. 2.3 V) at different folding states (Figure 5b), even when the device was folded by 180° (θ = 180°). To further understand the effect of deformation on the electrochemical performance of Na−O_2 batteries, galvanostatic discharge/charge measurements were conducted at different shapes. After being bent from 0 to 360°, the integrated flexible Na−O_2 battery still exhibits excellent cyclability with a reversible capacity of 1 Ah g^{-1} at 200 mA g^{-1} (based on the mass of Super P, Figures 5c and S35), which reveals the electrochemical stability of Na−O_2 batteries under external deformation.

CONCLUSIONS

In summary, a nonflammable QPE (PVdF−HFP−4% SiO_2−$NaClO_4$−TEGDME) with a high ionic conductivity of 1.0 mS cm^{-1} and good mechanical properties (Young's modulus ≈ 0.5 GPa) was developed for rechargeable Na−O_2 batteries. The unique porous structure and high dielectric constant induce the uniform distribution of electric field during the charge and discharge processes, ensuring the homogeneous deposition of Na. The excellent hydrophobic behavior and nonthrough nanopore structure of QPE could effectively protect the Na metal anode from H_2O erosion. Moreover, the enhanced liquid locking ability of QPE will avoid the possible leakage of an electrolyte. Therefore, the fabricated quasi-solid-state Na−O_2 batteries exhibit an average Coulombic efficiency of up to 97% and negligible voltage decay during 80 cycles at a discharge capacity of 1000 mAh g^{-1}. Furthermore, flexible Na−O_2 batteries show stable electrochemical performance for 400 h at various bending or folding states (0−360°). This work enlightens the application of a quasi-solid-state electrolyte and brings a new insight into the electrochemistry in rechargeable Na−O_2 batteries.

EXPERIMENTAL SECTION

Synthesis of QPE. PVdF−HFP polymer (2.0 g; Sigma-Aldrich) was dissolved in 20 mL of acetone with 4 wt % fumed silica (Sigma-Aldrich). The resultant solution was heated in an oil bath at 50 °C for 2 h with vigorous stirring, followed by resting at the same temperature for 1 h to make sure that no bubble remained. The solution was spread as a film on aluminum foil using a graduated blade. Then, the polymer film was dried at 80 °C in a vacuum oven. After cooling to room temperature, the polymer film was immersed into a pool of 1 M $NaClO_4$/TEGDME for at least 24 h. The moistened film was wiped with filter paper to remove the residual liquid electrolyte before use.

https://dx.doi.org/10.1021/acscentsci.0c00849
ACS Cent. Sci. 2020, 6, 1955−1963

Fabrication of Carbon Cathodes. The uniform slurry containing 1 g L^{-1} of commercial Super P nanoparticles in ethanol was sprayed onto one piece of carbon paper (Toray) or flexible carbon cloth (Fuel Cell Earth) that was supported by a wood board, dried at 100 °C for 10 h in a vacuum.

Materials Characterizations. The structures of QPE and the morphologies of the discharge products were observed by field-emission scanning electron microscopy (SEM, JEOL JSM7500F). Atomic force microscopy images and the roughness of QPE surface were collected on a Dimension Icon (Bruker) with Scan Asyst Mode. The morphology of SiO_2 was investigated by transmission electron microscopy (TEM, Philips Tecnai G2F-20). The components of QPE were detected by Fourier transform infrared spectroscopy (Thermo Nicolet MAGNA-IR 550 Spectrometer). Thermal gravimetric analyzer (TGA) curves come from a NETZSCH STA 449 F 3 Jupiter. The discharge products of Na−O_2 batteries were characterized by powder X-ray diffraction (Rigaku Mini-Flex600, Cu Kα radiation) and Raman spectroscopy. The Raman spectrum was collected on a Raman microscope (DXR Thermo Fisher Scientific) with excitation at 633 nm from an Ar-ion laser.

Electrochemical Measurements. The electrochemical performance of quasi-solid-state Na−O_2 batteries was tested at room temperature using CR2032 coin-type batteries. The batteries consist of a sodium metal anode, a QPE composite film containing 4% SiO_2 and $NaClO_4$/TEGDME (tetraethylene glycol dimethyl ether) electrolyte, and a Super P air cathode placed on a carbon paper supporter. While the electrochemical performance of flexible Na−O_2 batteries was tested, flexible carbon cloth was used as a cathode supporter. The cathode case was drilled to obtain several small pores for O_2 diffusion. All the batteries were assembled in a glovebox (Mikrouna Universal 2440/750) filled with argon. Then, all the assembled batteries were placed in a glovebox (Mikrouna Universal 2440/750) filled with high-purity O_2 with a pressure of 1 bar. The symmetric Na batteries were also assembled using a CR2032 coin-type battery model. After resting for 5 h, the batteries were subjected to galvanostatic discharge/charge on a LAND-CT2001A battery-testing system at room temperature. The ionic conductivity (σ) was calculated according to the equation of $\sigma = L/(RS)$, in which the electrolyte resistance (R) by electrochemical impedance spectroscopy (EIS), the membrane thickness (L), and the electrode area (S) were available. Cyclic voltammograms (CVs) were carried out on a CHI660E electrochemical workstation (CHI Instruments).

THEORETICAL CALCULATIONS

DFT Calculations. First-principles density functional theory (DFT) calculations were performed by using the Vienna ab initio simulation package (VASP).[48,49] Projector-augmented wave (PAW) pseudopotentials were adopted with an energy cutoff of 450 eV.[50] The generalized gradient approximation (GGA) and Perdew−Burke−Ernzerhof (PBE) functional were applied to both geometry optimization and self-consistent field computation.[51,52] All of the structural parameters were optimized until all force components were less than 0.02 eV $Å^{-1}$ and the convergence criterion of the total energy was 10^{-5} eV. The polymer chain was taken from the β-phase of PVdF crystals. A supercell that contains five monomers was prepared to simulate the polymer chain. Periodic boundary conditions were used with a lateral vacuum slab of 15 Å to ensure no interaction between neighboring chains. The electrostatic potentials diagram was calculated using quantitative analysis of the molecular surface in the open source Multiwfn package,[53,54] using the output file obtained from Gaussian 16 calculations.[55] The adsorption energy of Na atom on the PVdF is given by the equation

$$E_{ads} = E_{PVdF-Na} - E_{PVdF} - E_{Na}$$

where $E_{PVdF-Na}$, E_{PVdF}, and E_{Na} are the total energy of the PVdF chain with the adsorbed Na atom, the PVdF chain, and the Na atom, respectively. The migration barrier for Na^+ diffusion was obtained using the climbing image nudged elastic band (CI-NEB) method, where three images were used in the calculations.

Finite Element Simulations. Finite element method (FEM) was used to investigate the electrical field distribution around the surface of the Celgard separator and QPE. It was conducted by considering the physical models of electrostatics, which were based on the partial differential equations

$$E = -\nabla\varphi$$

$$\nabla\cdot(\varepsilon_0\varepsilon_r E) = \rho$$

where φ is the electric potential, E is the electric field, ε_0 is the vacuum dielectric constant, ε_r is the relative dielectric constant, and ρ is the charge density. The FEM simulations were performed in a rectangle area with a size of 28 by 70 μm for a Celgard separator system and a size of 210 nm by 70 μm for a QPE system. A Celgard separator was simplified as a sieve plate with a thickness of 50 μm and pore size of 4 μm, while QPE was a plate with a thickness of 50 μm and pore size of 30 nm. This simplified model can only be used to investigate the distribution difference of electric field strength resulting from the pore size and the dielectric constant of a Celgard separator and QPE. $\Delta\varphi$ is set as 0.02 V. The ε_r of the Celgard separator, TEGDME solvent, and PVdF−HFP are set as 2, 7.9, and 10, respectively.[56−58] Due to the complexity of the actual structure and distribution of pores in the QPE and Celgard separator, this model cannot fully reflect real circumstances. Thus, it was just used as a simplified ideal system to probe into the impact of pore size and dielectric constant of the Celgard separator and QPE on electric field distribution around the electrolyte surface. The only thing discussed here is whether smaller pore size and higher dielectric constant will result in a more even electric field distribution, which facilitates the uniform deposition of Na.

ASSOCIATED CONTENT

Supporting Information

The Supporting Information is available free of charge at https://pubs.acs.org/doi/10.1021/acscentsci.0c00849.

Figures S1−35 and Table S1 (PDF)

Video S1 (MP4)

AUTHOR INFORMATION

Corresponding Author

Jun Chen − *Key Laboratory of Advanced Energy Materials Chemistry (Ministry of Education), Renewable Energy Conversion and Storage Center (RECAST), College of Chemistry, Nankai University, Tianjin 310071, P.R. China;* orcid.org/0000-0001-8604-9689; Email: chenabc@nankai.edu.cn

https://dx.doi.org/10.1021/acscentsci.0c00849
ACS Cent. Sci. 2020, 6, 1955−1963

Authors

Jiaqi Wang − *Key Laboratory of Advanced Energy Materials Chemistry (Ministry of Education), Renewable Energy Conversion and Storage Center (RECAST), College of Chemistry, Nankai University, Tianjin 310071, P.R. China;* orcid.org/0000-0003-1176-704X

Youxuan Ni − *Key Laboratory of Advanced Energy Materials Chemistry (Ministry of Education), Renewable Energy Conversion and Storage Center (RECAST), College of Chemistry, Nankai University, Tianjin 310071, P.R. China*

Junxiang Liu − *Key Laboratory of Advanced Energy Materials Chemistry (Ministry of Education), Renewable Energy Conversion and Storage Center (RECAST), College of Chemistry, Nankai University, Tianjin 310071, P.R. China;* orcid.org/0000-0002-8256-1770

Yong Lu − *Key Laboratory of Advanced Energy Materials Chemistry (Ministry of Education), Renewable Energy Conversion and Storage Center (RECAST), College of Chemistry, Nankai University, Tianjin 310071, P.R. China*

Kai Zhang − *Key Laboratory of Advanced Energy Materials Chemistry (Ministry of Education), Renewable Energy Conversion and Storage Center (RECAST), College of Chemistry, Nankai University, Tianjin 310071, P.R. China;* orcid.org/0000-0001-8038-745X

Zhiqiang Niu − *Key Laboratory of Advanced Energy Materials Chemistry (Ministry of Education), Renewable Energy Conversion and Storage Center (RECAST), College of Chemistry, Nankai University, Tianjin 310071, P.R. China;* orcid.org/0000-0001-9560-7283

Complete contact information is available at: https://pubs.acs.org/10.1021/acscentsci.0c00849

Author Contributions

The manuscript was written through contributions of all authors. All authors have given approval to the final version of the manuscript.

Author Contributions

[†]J.W. and Y.N. contributed equally to this work.

Notes

The authors declare no competing financial interest.

■ ACKNOWLEDGMENTS

This work was supported by the National Programs for Nano-Key Project (2017YFA0206700), the National Natural Science Foundation of China (21835004), and the 111 Project from the Ministry of Education of China (B12015). The calculations in this work were performed on TianHe-1(A), National Supercomputer Center in Tianjin.

■ REFERENCES

(1) Hartmann, P.; Bender, C. L.; Vračar, M.; Dürr, A. K.; Garsuch, A.; Janek, J.; Adelhelm, P. A rechargeable room-temperature sodium superoxide (NaO_2) battery. *Nat. Mater.* **2013**, *12*, 228−232.

(2) Xu, J.-J.; Chang, Z.-W.; Yin, Y.-B.; Zhang, X.-B. Nanoengineered ultralight and robust all-metal cathode for high-capacity, stable lithium−oxygen batteries. *ACS Cent. Sci.* **2017**, *3*, 598−604.

(3) Yadegari, H.; Sun, Q.; Sun, X. Sodium-Oxygen Batteries: A Comparative Review from Chemical and Electrochemical Fundamentals to Future Perspective. *Adv. Mater.* **2016**, *28*, 7065−7093.

(4) Das, S. K.; Lau, S.; Archer, L. A. Sodium−oxygen batteries: a new class of metal−air batteries. *J. Mater. Chem. A* **2014**, *2*, 12623−12629.

(5) Zhao, Q.; Yan, Z.; Chen, C.; Chen, J. Spinels: Controlled Preparation, Oxygen Reduction/Evolution Reaction Application, and Beyond. *Chem. Rev.* **2017**, *117*, 10121−10211.

(6) Tang, X.; Zhou, D.; Li, P.; Guo, X.; Wang, C.; Kang, F.; Li, B.; Wang, G. High-Performance Quasi-Solid-State MXene-Based Li−I Batteries. *ACS Cent. Sci.* **2019**, *5*, 365−373.

(7) McCloskey, B. D.; Garcia, J. M.; Luntz, A. C. Chemical and electrochemical differences in nonaqueous $Li-O_2$ and $Na-O_2$ batteries. *J. Phys. Chem. Lett.* **2014**, *5*, 1230−1235.

(8) Sun, B.; Pompe, C.; Dongmo, S.; Zhang, J.; Kretschmer, K.; Schröder, D.; Janek, J.; Wang, G. Challenges for Developing Rechargeable Room-Temperature Sodium Oxygen Batteries. *Adv. Mater. Technol.* **2018**, *3*, 1800110.

(9) Kwak, W. J.; Chen, Z.; Yoon, C. S.; Lee, J. K.; Amine, K.; Sun, Y. K. Nanoconfinement of low-conductivity products in rechargeable sodium−air batteries. *Nano Energy* **2015**, *12*, 123−130.

(10) Landa-Medrano, I.; Pinedo, R.; Bi, X.; Ruiz de Larramendi, I.; Lezama, L.; Janek, J.; Amine, K.; Lu, J.; Rojo, T. New insights into the instability of discharge products in $Na-O_2$ batteries. *ACS Appl. Mater. Interfaces* **2016**, *8*, 20120−20127.

(11) Chi, X.; Hao, F.; Zhang, J.; Wu, X.; Zhang, Y.; Gheytani, S.; Wen, Z.; Yao, Y. A high-energy quinone-based all-solid-state sodium metal battery. *Nano Energy* **2019**, *62*, 718−724.

(12) Zhao, Y.; Goncharova, L. V.; Lushington, A.; Sun, Q.; Yadegari, H.; Wang, B.; Xiao, W.; Li, R.; Sun, X. Superior stable and long life sodium metal anodes achieved by atomic layer deposition. *Adv. Mater.* **2017**, *29*, 1606663.

(13) Tian, H.; Seh, Z. W.; Yan, K.; Fu, Z.; Tang, P.; Lu, Y.; Zhang, R.; Legut, D.; Cui, Y.; Zhang, Q. Theoretical investigation of 2D layered materials as protective films for lithium and sodium metal anodes. *Adv. Energy Mater.* **2017**, *7*, 1602528.

(14) Lu, Y.; Cai, Y.; Zhang, Q.; Liu, L.; Niu, Z.; Chen, J. A compatible anode/succinonitrile-based electrolyte interface in all-solid-state $Na-CO_2$ batteries. *Chem. Sci.* **2019**, *10*, 4306−4312.

(15) Lee, B.; Paek, E.; Mitlin, D.; Lee, S. W. Sodium Metal Anodes: Emerging Solutions to Dendrite Growth. *Chem. Rev.* **2019**, *119*, 5416−5460.

(16) Shi, Q.; Zhong, Y.; Wu, M.; Wang, H.; Wang, H. High-Performance Sodium Metal Anodes Enabled by a Bifunctional Potassium Salt. *Angew. Chem.* **2018**, *130*, 9207−9210.

(17) Wu, S.; Qiao, Y.; Jiang, K.; He, Y.; Guo, S.; Zhou, H. Tailoring Sodium Anodes for Stable Sodium-Oxygen Batteries. *Adv. Funct. Mater.* **2018**, *28*, 1706374.

(18) Gao, H.; Xin, S.; Xue, L.; Goodenough, J. B. Stabilizing a high-energy-density rechargeable sodium battery with a solid electrolyte. *Chem.* **2018**, *4*, 833−844.

(19) Zhou, W.; Li, Y.; Xin, S.; Goodenough, J. B. Rechargeable sodium all-solid-state battery. *ACS Cent. Sci.* **2017**, *3*, 52−57.

(20) Wang, L.; Pan, J.; Zhang, Y.; Cheng, X.; Liu, L.; Peng, H. A Li-Air Battery with Ultralong Cycle Life in Ambient Air. *Adv. Mater.* **2018**, *30*, 1704378.

(21) Yin, Y. B.; Yang, X. Y.; Chang, Z. W.; Zhu, Y. H.; Liu, T.; Yan, J. M.; Jiang, Q. A Water-/Fireproof Flexible Lithium-Oxygen Battery Achieved by Synergy of Novel Architecture and Multifunctional Separator. *Adv. Mater.* **2018**, *30*, 1703791.

(22) Costa, C. M.; Silva, M. M.; Lanceros-Méndez, S. Battery separators based on vinylidenefluoride (VDF) polymers and copolymers for lithium ion battery applications. *RSC Adv.* **2013**, *3*, 11404−11417.

(23) Sun, J.; Lu, Y.; Yang, H.; Han, M.; Shao, L.; Chen, J. Rechargeable $Na-CO_2$ Batteries Starting from Cathode of Na_2CO_3 and Carbon Nanotubes. *Research* **2018**, *2018*, 6914626.

(24) Ma, J.; Meng, F.; Yu, Y.; Liu, D.; Yan, J.; Zhang, Y.; Zhang, X.; Jiang, Q. Prevention of dendrite growth and volume expansion to give high-performance aprotic bimetallic Li-Na alloy−O_2 batteries. *Nat. Chem.* **2019**, *11*, 64−70.

(25) Sun, B.; Li, P.; Zhang, J.; Wang, D.; Munroe, P.; Wang, C.; Notten, P.; Wang, G. Dendrite-Free Sodium-Metal Anodes for High-Energy Sodium-Metal Batteries. *Adv. Mater.* **2018**, *30*, 1801334.

(26) Ma, J.; Yin, Y.; Liu, T.; Zhang, X.; Yan, J.; Jiang, Q. Suppressing Sodium Dendrites by Multifunctional Polyvinylidene Fluoride (PVDF) Interlayers with Nonthrough Pores and High Flux/Affinity of Sodium Ions toward Long Cycle Life Sodium Oxygen-Batteries. *Adv. Funct. Mater.* **2018**, *28*, 1703931.
(27) He, X.; Shi, Q.; Zhou, X.; Wan, C.; Jiang, C. In situ composite of nano SiO_2-P(VDF-HFP) porous polymer electrolytes for Li-ion batteries. *Electrochim. Acta* **2005**, *51*, 1069−1075.
(28) Liu, Z.; Li, H.; Zhu, M.; Huang, Y.; Tang, Z.; Pei, Z.; Wang, Z.; Shi, Z.; Liu, J.; Huang, Y.; Zhi, C. Towards wearable electronic devices: A quasi-solid-state aqueous lithium-ion battery with outstanding stability, flexibility, safety and breathability. *Nano Energy* **2018**, *44*, 164−173.
(29) Zhang, D.; Li, R.; Huang, T.; Yu, A. Novel composite polymer electrolyte for lithium air batteries. *J. Power Sources* **2010**, *195*, 1202−1206.
(30) Genzer, J.; Efimenko, K. Creating long-lived superhydrophobic polymer surfaces through mechanically assembled monolayers. *Science* **2000**, *290*, 2130−2133.
(31) Hu, X.; Li, Z.; Zhao, Y.; Sun, J.; Zhao, Q.; Wang, J.; Tao, Z.; Chen, J. Quasi-solid state rechargeable Na-CO_2 batteries with reduced graphene oxide Na anodes. *Sci. Adv.* **2017**, *3*, e1602396.
(32) Aravindan, V.; Lakshmi, C.; Vickraman, P. Investigations on Na^+ ion conducting polyvinylidenefluoride-co-hexafluoro-propylene/poly ethylmethacrylate blend polymer electrolytes. *Curr. Appl. Phys.* **2009**, *9*, 1106−1111.
(33) Zhu, Z.; Hong, M.; Guo, D.; Shi, J.; Tao, Z.; Chen, J. All-solid-state lithium organic battery with composite polymer electrolyte and pillar[5]quinone cathode. *J. Am. Chem. Soc.* **2014**, *136*, 16461−16464.
(34) Tan, R.; Gao, R.; Zhao, Y.; Zhang, M.; Xu, J.; Yang, J.; Pan, F. Novel organic−inorganic hybrid electrolyte to enable $LiFePO_4$ quasi-solid-state Li-ion batteries performed highly around room temperature. *ACS Appl. Mater. Interfaces* **2016**, *8*, 31273−31280.
(35) Zhao, C.-Z.; Chen, P.-Y.; Zhang, R.; Chen, X.; Li, B.-Q.; Zhang, X.-Q.; Cheng, X.-B.; Zhang, Q. An ion redistributor for dendrite-free lithium metal anodes. *Sci. Adv.* **2018**, *4*, eaat3446.
(36) Zhang, K.; Lee, G. H.; Park, M.; Li, W.; Kang, Y. M. Recent developments of the lithium metal anode for rechargeable non-aqueous batteries. *Adv. Energy Mater.* **2016**, *6*, 1600811.
(37) Ding, F.; Xu, W.; Graff, G. L.; Zhang, J.; Sushko, M. L.; Chen, X.; Shao, Y.; Engelhard, M. H.; Nie, Z.; Xiao, J.; Liu, X.; Sushko, P. V.; Liu, J.; Zhang, J.-G. Dendrite-free lithium deposition via self-healing electrostatic shield mechanism. *J. Am. Chem. Soc.* **2013**, *135*, 4450−4456.
(38) Zhao, Y.; Goncharova, L. V.; Lushington, A.; Sun, Q.; Yadegari, H.; Wang, B.; Xiao, W.; Li, R.; Sun, X. Superior stable and long life sodium metal anodes achieved by atomic layer deposition. *Adv. Mater.* **2017**, *29*, 1606663.
(39) Barai, P.; Higa, K.; Srinivasan, V. Lithium dendrite growth mechanisms in polymer electrolytes and prevention strategies. *Phys. Chem. Chem. Phys.* **2017**, *19*, 20493−20505.
(40) Wang, J.; Liu, J.; Cai, Y.; Cheng, F.; Niu, Z.; Chen, J. Super P Carbon Modified Lithium Anode for High-Performance Li-O_2 Batteries. *ChemElectroChem* **2018**, *5*, 1702−1707.
(41) Harry, K. J.; Higa, K.; Srinivasan, V.; Balsara, N. P. Influence of electrolyte modulus on the local current density at a dendrite tip on a lithium metal electrode. *J. Electrochem. Soc.* **2016**, *163*, A2216−A2224.
(42) Xia, C.; Black, R.; Fernandes, R.; Adams, B.; Nazar, L. F. The critical role of phase-transfer catalysis in aprotic sodium oxygen batteries. *Nat. Chem.* **2015**, *7*, 496−501.
(43) Liu, J.; Wang, J.; Ni, Y.; Zhang, Y.; Luo, J.; Cheng, F.; Chen, J. Spinel/Lithium-Rich Manganese Oxide Hybrid Nanofibers as Cathode Materials for Rechargeable Lithium-Ion Batteries. *Small Methods* **2019**, *3*, 1900350.
(44) Liu, T.; Kim, G.; Casford, M. T.; Grey, C. P. Mechanistic insights into the challenges of cycling a nonaqueous Na−O_2 battery. *J. Phys. Chem. Lett.* **2016**, *7*, 4841−4846.
(45) Sun, B.; Kretschmer, K.; Xie, X.; Munroe, P.; Peng, Z.; Wang, G. Hierarchical Porous Carbon Spheres for High-Performance Na-O_2 Batteries. *Adv. Mater.* **2017**, *29*, 1606816.
(46) Kim, J.; Park, H.; Lee, B.; Seong, W. M.; Lim, H. D.; Bae, Y.; Kim, H.; Kim, W. K.; Ryu, K. H.; Kang, K. Dissolution and ionization of sodium superoxide in sodium−oxygen batteries. *Nat. Commun.* **2016**, *7*, 10670.
(47) Ortiz-Vitoriano, N.; Batcho, T. P.; Kwabi, D. G.; Han, B.; Pour, N.; Yao, K. P. C.; Thompson, C. V.; Shao-Horn, Y. Rate-dependent nucleation and growth of NaO_2 in Na−O_2 batteries. *J. Phys. Chem. Lett.* **2015**, *6*, 2636−2643.
(48) Kresse, G.; Furthmüller, J. Efficiency of ab-initio total energy calculations for metals and semiconductors using a plane-wave basis set. *Comput. Mater. Sci.* **1996**, *6*, 15−50.
(49) Kresse, G.; Furthmüller, J. Efficient iterative schemes for ab initio total-energy calculations using a plane-wave basis set. *Phys. Rev. B: Condens. Matter Mater. Phys.* **1996**, *54*, 11169−11186.
(50) Blöchl, P. E. Projector augmented-wave method. *Phys. Rev. B: Condens. Matter Mater. Phys.* **1994**, *50*, 17953−17979.
(51) Perdew, J. P.; Burke, K.; Ernzerhof, M. Generalized gradient approximation made simple. *Phys. Rev. Lett.* **1996**, *77*, 3865−3868.
(52) Perdew, J. P.; Wang, Y. Pair-distribution function and its coupling-constant average for the spin-polarized electron gas. *Phys. Rev. B: Condens. Matter Mater. Phys.* **1992**, *46*, 12947−12954.
(53) Lu, T.; Chen, F. Multiwfn: a multifunctional wavefunction analyzer. *J. Comput. Chem.* **2012**, *33*, 580−592.
(54) Lu, T.; Chen, F. Quantitative analysis of molecular surface based on improved Marching Tetrahedra algorithm. *J. Mol. Graphics Modell.* **2012**, *38*, 314−323.
(55) Frisch, M. J.; Trucks, G. W.; Schlegel, H. B.; Scuseria, G. E.; Robb, M. A.; Cheeseman, J. R.; Scalmani, G.; Barone, V.; Petersson, G. A.; Nakatsuji, H.; Li, X.; Caricato, M.; Marenich, A. V.; Blolino, J.; Janesko, B. G.; Gomperts, R.; Mennucci, B.; Hratchian, H. P.; Ortiz, J. V.; Izmaylov, A. F.; Sonnenberg, J. L.; Williams-Young, D.; Ding, F.; Lipparini, F.; Egidi, F.; Goings, J.; Peng, B.; Petrone, A.; Henderson, T.; Ranasinghe, D.; Zakrzewski, V. G.; Gao, J.; Rega, N.; Zheng, G.; Liang, W.; Hada, M.; Ehara, M.; Toyota, K.; Fukuda, R.; Hasegawa, J.; Ishida, M.; Nakajima, T.; Honda, Y.; Kitao, O.; Nakai, H.; Vreven, T.; Throssell, K.; Montgomery, J. A., Jr.; Peralta, J. E.; Oligaro, F.; Bearpark, M. J.; Heyd, J. J; Brothers, E. N.; Kudin, K. N.; Staroverov, V. N.; Keith, T. A.; Kobayashi, R.; Normand, J.; Ragavachari, K.; Rendell, A. P.; Burant, J. C.; Iyengar, S. S.; Tomasi, J.; Cossi, M.; Millam, J. M.; Klene, M.; Adamo, C.; Cammi, R.; Ochterski, J. W.; Martin, R. L.; Morokuma, K.; Farkas, O.; Foresman, J. B.; Fox, D. J. *Gaussian 16*, revision A.02; Gaussian, Inc.: Wallingford, CT, 2016.
(56) Tjong, S. C.; Liang, G. D.; Bao, S. P. Electrical behavior of polypropylene/multiwalled carbon nanotube nanocomposites with low percolation threshold. *Scr. Mater.* **2007**, *57*, 461−464.
(57) Barchasz, C.; Leprêtre, J. C.; Patoux, S.; Alloin, F. Electrochemical properties of ether-based electrolytes for lithium/sulfur rechargeable batteries. *Electrochim. Acta* **2013**, *89*, 737−743.
(58) Liu, Z. D.; Feng, Y.; Li, W. L. High dielectric constant and low loss of polymeric dielectric composites filled by carbon nanotubes adhering $BaTiO_3$ hybrid particles. *RSC Adv.* **2015**, *5*, 29017−29021.

https://dx.doi.org/10.1021/acscentsci.0c00849
ACS Cent. Sci. 2020, 6, 1955−1963